Alignment of the projectile $2p_{3/2}$ state created by nonradiative electron capture in 95- and 146-MeV/u Xe^{54+} with Kr and Xe collisions

Bian Yang [1,2] Deyang Yu [1,2,*] Caojie Shao [1,2] Yury S. Kozhedub [3] Yingli Xue [1,2] Wei Wang [1,2] Mingwu Zhang [1]
Junliang Liu [1,2] Zhangyong Song [1,2] Rongchun Lu,[1,2] Fangfang Ruan,[4] Yehong Wu,[5] and Xiaohong Cai[1,2]

[1]*Institute of Modern Physics, Chinese Academy of Sciences, Lanzhou 730000, China*
[2]*University of Chinese Academy of Sciences, Beijing 100049, China*
[3]*Department of Physics, Saint Petersburg State University, Saint Petersburg 199034, Russia*
[4]*Department of Medical Imaging, Hangzhou Medical College, Hangzhou 310053, China*
[5]*School of Basic Medical Sciences, Shanxi Medical University, Taiyuan 030001, China*

Anisotropic distributions of the Lyman-α_1 transition of the down-charged Xe^{53+*} ions are observed in fast Xe^{54+} with Kr and Xe collisions, in which the electron is transferred by the nonradiative electron capture mechanism. At the energy of 95 MeV/u, the alignment parameter of the projectile $2p_{3/2}$ state, $\mathcal{A}_{20}$, is determined to be -0.35 ± 0.02 for both targets. While the projectile energy is 146 MeV/u, the parameter for the Kr and Xe target is -0.28 ± 0.02 and -0.29 ± 0.04, respectively. The present results demonstrate that the electron capture to the $m_j = \pm 1/2$ magnetic substates is about two times more probable than to the $m_j = \pm 3/2$ ones.

I. INTRODUCTION

Electron capture is a basic process in ion-atom collisions, and plays a significant role in many branches of physics, such as plasma and astrophysics [1–3]. There are two competing mechanisms of the single-electron capture in fast ion-atom collisions, i.e., the radiative electron capture (REC) and the nonradiative electron capture (NRC) [4,5]. In the REC mechanism, a target electron transfers into a bound state of the ion, while the conservations of energy and momentum are achieved by emitting a photon. In the NRC case, the relative motion between the two nuclei is modified by exchange of the transferred electron, and hence energy and momentum are conserved. Essentially, competition between REC and NRC depends on the comparison between the electron−free-electromagnetic-field interaction and the electron-nuclei interaction. In high-energy collisions, the cross sections of REC and NRC roughly follow the scaling laws [4,5] of $\sigma^{\mathrm{REC}} \propto Z_{\mathrm{P}}^5 Z_{\mathrm{T}}/E_{\mathrm{P}}$ and $\sigma^{\mathrm{NRC}} \propto Z_{\mathrm{P}}^5 Z_{\mathrm{T}}^5/E_{\mathrm{P}}$, respectively. Here E_{P} is the projectile energy, and Z_{P} and Z_{T} are the atomic numbers of the projectile ion and the target atom, respectively. Usually, the REC channel dominates for loosely bounded outer-shell target electrons in the relativistic energy regime. In contrast, transfer of tightly bounded inner-shell electrons at nonrelativistic energies is mostly due to the NRC mechanism.

In the projectile frame, the target electrons on average have a certain momentum which is antiparallel to the ion-beam direction, as well as an orbital angular momentum which is perpendicular to this momentum. Thus, the initial orbital angular momentum of the target electrons is nearly in the plane

which is perpendicular to the ion-beam direction, rather than isotropic in all directions. Therefore, when a target electron is captured into an excited state with total angular momentum $J > \frac{1}{2}$ (e.g., the $2p_{3/2}$ state), population of magnetic substates tends to deviate from the statistical distribution (i.e., to be aligned or polarized). Subsequently, this will result in both polarization [5,6] and anisotropic distribution [5,7] of the emitted photons when this excited state decays.

A few experiments have been devoted to the alignment effect in NRC processes concerning energetic highly charged ions. Pedersen *et al.* [8] studied the collisions of 1.74-MeV/u F^{9+} ions with Ar atoms, Ellsworth *et al.* [9] studied bare ions with $6 \leqslant Z_{\mathrm{P}} \leqslant 9$ incident on helium around MeV/u energies, and later Wohrer *et al.* [10] investigated Kr^{36+} colliding with Ne, Ar, and Kr atoms at 33 MeV/u. In these works, anisotropic angular distribution of the projectile Lyman x rays was observed and attributed to the alignment of the excited down-charged ions. However, the alignment parameter of the $2p_{3/2}$ state has not been obtained since the Lyman-α_1 ($2p_{3/2} \rightarrow 1s_{1/2}$) transition was blurred by the Lyman-α_2 ($2p_{1/2} \rightarrow 1s_{1/2}$) line. Church *et al.* [11] and Pálinkás *et al.* [12,13] employed 2–3-MeV/u Mg and S ions to pass through carbon foils, and observed anisotropic distributions of the projectile K x rays. The anisotropy was attributed to the alignment of the K-shell vacancy states, which were created by projectile excitation, as well as the striping and capture processes, during the penetration. Theoretically, the first-order continuum distorted wave approximation provided a good agreement with the experiment [14–16] in high-energy collisions.

Recently, heavy-ion storage rings have offered us bare heavy-ion beams, and then enabled us to investigate their collisions with atoms experimentally at projectile energies around a few hundred MeV/u. In these collisions, the alignment effect has been investigated, both experimentally and
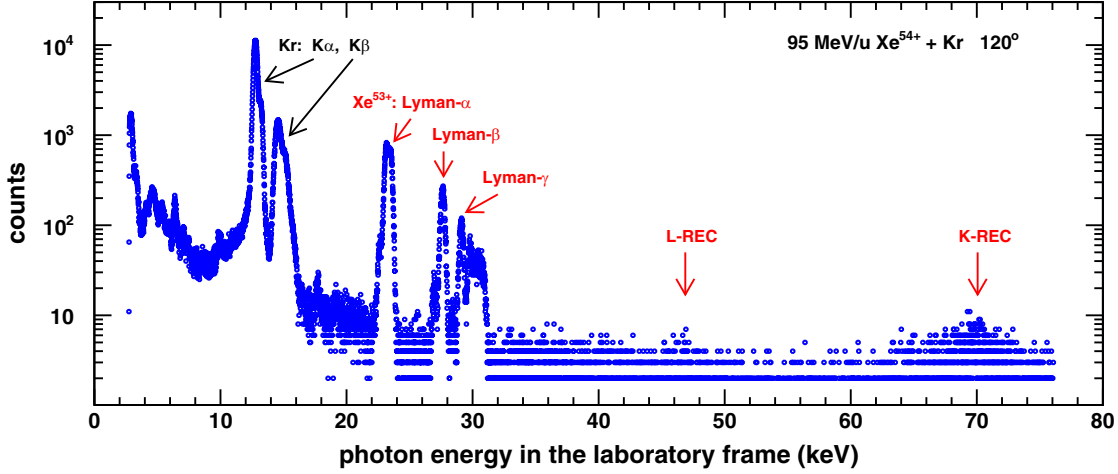
_____
*Corresponding author: d.yu@impcas.ac.cn

FIG. 1. X-ray spectrum obtained from the HPGe detector at an observation angle of 120° relative to the ion-beam direction in collisions of 95-MeV/u Xe^{54+} ions with Kr atoms.

theoretically, in channels of REC [5–7,17–23], resonant transfer excitation [24–26], projectile excitation [27,28], and simultaneous projectile excitation and ionization [29,30].

In this paper, we report anisotropic distributions of the Lyman-α_1 transition of the down-charged Xe^{53+*} ions in 95- and 146-MeV/u Xe^{54+} with Kr and Xe collisions. The alignment parameter $\mathcal{A}_{20}$ of the projectile $2p_{3/2}$ state produced by the NRC mechanism is determined. The experiment and the data analysis are described in the next section. The physical results and discussion are presented in Sec. III, and finally a summary is given in Sec. IV.

II. EXPERIMENT AND DATA ANALYSIS

The experiment was carried out at the experimental ring (CSRe) of the Heavy Ion Research Facility at Lanzhou–Cooling Storage Ring [31,32]. The experimental setup and procedures have been described elsewhere [33]. Briefly, Xe^{54+} ions of 95 and 146 MeV/u, stored and electron cooled in CSRe, were employed to collide with atomic beams [34,35] of Kr and Xe, respectively. The ion-beam intensity was about 100–600 μA, and the relative momentum spread was kept around 2–5×10^{-5}. The target thickness is estimated to be 10^{12-13} atoms/cm^2, and therefore the single-collision condition is well satisfied according to the total single-capture cross section of around 10^{-20} cm^2 in the present experiment [36–38]. X rays emitted from the interaction region were detected by four high-purity germanium (HPGe) detectors and two lithium-drifted silicon detectors, which were placed at 35°, 60°, 90°, 120°, and 145° observation angles to the ion-beam direction, respectively. Typical energy resolution (i.e., the full width at half maximum) of these detectors is about 300 eV in the interested region. The signals from the detectors were processed by standard Nuclear Instrument Module electronics and recorded by a commercial multiparameter multichannel analyzer (FAST model MPA-3). The detection system was calibrated by using ^{55}Fe, ^{133}Ba, ^{152}Eu, and ^{241}Am radioactive sources before and after the experiment [33].

Figure 1 shows an example x-ray spectrum registered at a beam energy of 95 MeV/u by an HPGe detector placed at an observation angle of 120° for Xe^{54+} with Kr collisions. The x-ray spectra corresponding to the target $K\alpha$ and $K\beta$ lines, as well as the Doppler-shifted projectile Lyman and Balmer lines, dominate the spectrum. Figure 2 shows typical projectile x-ray spectra obtained in the collisions between 95-MeV/u Xe^{54+} and Kr, at observation angles of 35°, 60°, 90°, 120°, and 145°. The photon energy has been calibrated to the projectile frame, according to the Doppler effect. The energy range has been zoomed in to the projectile Lyman-α region. Besides the singly down-charged ions Xe^{53+*}, the doubly down-charged ions Xe^{52+*} contribute to the spectra also. At each observation angle, the intensity ratios between the Lyman-α_1 transition $2p_{3/2} \rightarrow 1s_{1/2}$ and the Lyman-α_2 transition $2p_{1/2} \rightarrow 1s_{1/2}$ (mixed with the $M1$ transition $2s_{1/2} \rightarrow 1s_{1/2}$) of the Xe^{53+*} ions are obtained by a multipeak (with linear background) fitting procedure, and also are shown in Fig. 2.

In the collisions between both unpolarized partners, the states with the total angular momentum of $J = \frac{1}{2}$ (e.g., the $2p_{1/2}$ and $2s_{1/2}$ states) cannot be aligned [5,7]. Therefore, the Lyman-α_2 transition $2p_{1/2} \rightarrow 1s_{1/2}$ and the $M1$ transition $2s_{1/2} \rightarrow 1s_{1/2}$ of the Xe^{53+*} ions are isotropic in the projectile frame. According to the Lorentz transformation, the angular distribution of these transitions in the laboratory frame [39] satisfies

$$\frac{d\sigma_{\text{Ly-}\alpha_2(+M1)}}{d\Omega}(\theta_{\text{lab}}) = \frac{\sigma_{\text{Ly-}\alpha_2(+M1)}^{\text{total}}}{4\pi} \frac{1 - \beta^2}{(1 - \beta \cos\theta_{\text{lab}})^2}, \quad (1)$$

where θ_{lab} is the angle between the directions of the projectile and the emitted photon in the laboratory frame [5,40], β is the reduced projectile velocity in the unit of light speed, and $\sigma_{\text{Ly-}\alpha_2(+M1)}^{\text{total}}$ denotes the total cross section of the Lyman-α_2 and $M1$ transitions.

In contrast, the $2p_{3/2}$ state of the down-charged Xe^{53+*} ions can be aligned in the present collisions. Therefore, the angular distribution of the Lyman-α_1 transition in the projectile frame is anisotropic. It can be described as [5,7,39]

$$\frac{d\sigma_{\text{Ly-}\alpha_1}}{d\Omega}(\theta_{\text{proj}}) = \frac{\sigma_{\text{Ly-}\alpha_1}^{\text{total}}}{4\pi}\left[1 + \beta_{20}\left(1 - \frac{3}{2}\sin^2\theta_{\text{proj}}\right)\right], \quad (2)$$
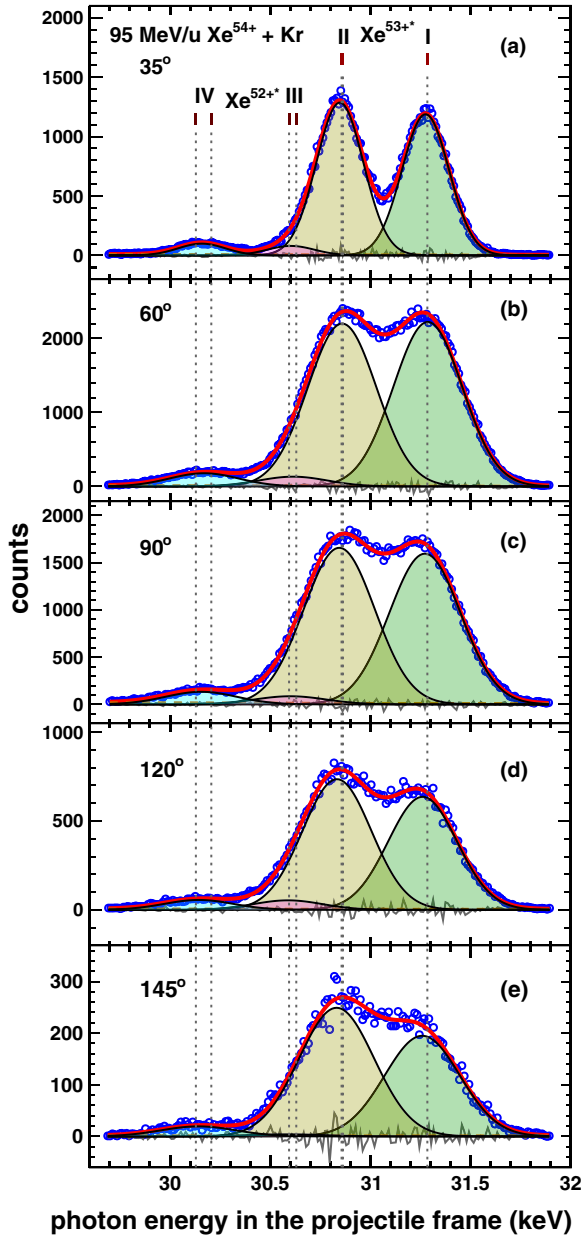
FIG. 2. X-ray spectra of the K-shell radiation from Xe^{53+*} and Xe^{52+*} produced in collisions of 95-MeV/u Xe^{54+} with Kr at observation angles of (a) 35°, (b) 60°, (c) 90°, (d) 120°, and (e) 145°. The peaks marked as I and II correspond to the transitions of Lyman-α_1 ($2p_{3/2} \rightarrow 1s_{1/2}$) and Lyman-$\alpha_2$ ($2p_{1/2} \rightarrow 1s_{1/2}$, which is mixed with $2s_{1/2} \rightarrow 1s_{1/2}$) of the down-charged Xe^{53+*} ions, respectively. The peaks III and IV are the radiations of $(1s_{1/2}2p_{3/2})_1 \rightarrow 1s^2$ [mixed with $(1s_{1/2}2p_{3/2})_2 \rightarrow 1s^2$] and $(1s_{1/2}2p_{1/2})_1 \rightarrow 1s^2$ [mixed with $(1s_{1/2}2s_{1/2})_1 \rightarrow 1s^2$] from the doubly down-charged Xe^{52+*} ions, respectively. The energies of these transitions are illustrated by dashed vertical lines. Areas of these peaks are determined by a multipeak (with linear background) fitting procedure. The fitting residuals are also shown.

where θ_{proj} is the angle between the directions of the emitted photon and the target atom in the projectile frame, and $\sigma_{\text{Ly-}\alpha_1}^{\text{total}}$

is the total cross section of the Lyman-α_1 transition. Here,

$$\beta_{20} = \alpha \mathcal{A}_{20} = \alpha \frac{\sigma\left(\frac{3}{2}, \pm\frac{3}{2}\right) - \sigma\left(\frac{3}{2}, \pm\frac{1}{2}\right)}{\sigma\left(\frac{3}{2}, \pm\frac{3}{2}\right) + \sigma\left(\frac{3}{2}, \pm\frac{1}{2}\right)} \tag{3}$$

is the anisotropy parameter of the Lyman-α_1 transition, and $\mathcal{A}_{20}$ is the alignment parameter of the $2p_{3/2}$ state. The symbol $\sigma(j, m_j)$ denotes the population of the magnetic substate of angular momentum j and its projection on the projectile direction, m_j. It should be noted that the population $\sigma(j, m_j)$ always equals to $\sigma(j, -m_j)$ when both collisional partners are unpolarized [5]. If only the leading $E1$ transition is considered, the coefficient α equals $1/2$ for the Lyman-α_1 decay [5,7]. When the $M2$ transition is taken into account, the interference effect modifies the coefficient and results in $\alpha_{\text{eff}} = 0.545$ for the case of hydrogenlike Xe ions [20,41]. In the laboratory frame, this front-back symmetric distribution [e.g., Eq. (2)] is distorted by the Lorentz transformation [7,39]:

$$\frac{d\sigma_{\text{Ly-}\alpha_1}}{d\Omega}(\theta_{\text{lab}}) = \frac{\sigma_{\text{Ly-}\alpha_1}^{\text{total}}}{4\pi} \frac{1 - \beta^2}{(1 - \beta\cos\theta_{\text{lab}})^2}$$
$$\times \left\{1 + \beta_{20}\left[1 - \frac{3}{2}\frac{(1-\beta^2)\sin^2\theta_{\text{lab}}}{(1-\beta\cos\theta_{\text{lab}})^2}\right]\right\}. \tag{4}$$

The intensity ratio between the Lyman-α_1 and Lyman-α_2 ($+M1$) transitions, as a function of the observation angle θ_{lab},

$$\frac{I_{\text{Ly-}\alpha_1}(\theta_{\text{lab}})}{I_{\text{Ly-}\alpha_2(+M1)}(\theta_{\text{lab}})} = \frac{\sigma_{\text{Ly-}\alpha_1}^{\text{total}}}{\sigma_{\text{Ly-}\alpha_2(+M1)}^{\text{total}}}$$
$$\times \left\{1 + \beta_{20}\left[1 - \frac{3}{2}\frac{(1-\beta^2)\sin^2\theta_{\text{lab}}}{(1-\beta\cos\theta_{\text{lab}})^2}\right]\right\},$$
$$\tag{5}$$

is employed to deduce the total cross-section ratio $\sigma_{\text{Ly-}\alpha_1}^{\text{total}}/\sigma_{\text{Ly-}\alpha_2(+M1)}^{\text{total}}$ and the anisotropy parameter β_{20} by fitting experimental data [7]. Here, the transitions $2p_{1/2} \rightarrow 1s_{1/2}$ and $2s_{1/2} \rightarrow 1s_{1/2}$ serve as the standard of isotropic distribution. By this means, a possible systematic uncertainty originated from the solid angles of detectors is canceled out. Furthermore, because the transition energies of the Lyman-α_1, Lyman-α_2, and $M1$ are close to each other, the uncertainty resulting from the difference of the detection efficiencies is also suppressed.

III. RESULTS AND DISCUSSION

The intensity ratios between the Lyman-α_1 and the Lyman-α_2 together with the $M1$ transitions at 35°, 60°, 90°, 120°, and 145°, measured in the collisions of Xe^{54+} with Kr and Xe at 95 and 146 MeV/u, and fitted by curves according to Eq. (5), are shown in Fig. 3. Significant anisotropic distributions of the Lyman-α_1 transition are observed for both targets at each collision energy. As listed in Table I, the population ratio between the $m_j = \pm1/2$ magnetic substates and the $m_j = \pm3/2$ substates is as high as around 2.1 for both targets at 95 MeV/u, and around 1.8 for both targets at 146 MeV/u. These values considerably deviate from the statistical (equal) population and lead to emission of strongly polarized Lyman-α_1 photons. It also implies that the emission of Lyman-α_1 photons occurs preferentially perpendicular to the beam
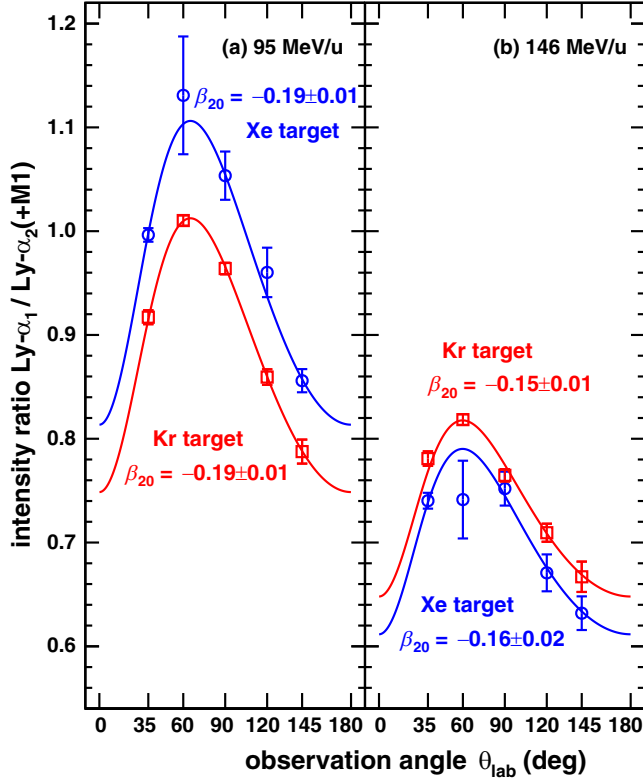
FIG. 3. Angular distributions of the Lyman-α_1 ($2p_{3/2} \to 1s_{1/2}$) transition of the Xe^{53+*} ions produced in collisions of Xe^{54+} with Kr (red open squares) and Xe (blue open circles). The projectile energy is (a) 95 MeV/u and (b) 146 MeV/u. The intensity of Lyman-α_1 is normalized by the Lyman-α_2 ($2p_{1/2} \to 1s_{1/2}$) and the $M1$ ($2s_{1/2} \to 1s_{1/2}$) transitions, which are isotropic in the projectile frame. The solid lines are fittings of the experimental data according to Eq. (5). The fitting parameters, as well some deduced results, are collected in Table I. The large error bars of the Xe target are originated from overlap between the projectile Lyman-α lines and the target K x rays.

direction. Moreover, we note a rather weak target species, but remarkable projectile energy dependency of the alignment effect, which increases with decreasing collision energy. The cross-section ratio $\sigma_{\text{Ly-}\alpha_1}^{\text{total}}/\sigma_{\text{Ly-}\alpha_2(+M1)}^{\text{total}}$ represents the population ratio between the $2p_{3/2}$ and the $2p_{1/2}$ (together with $2s_{1/2}$) states. The results presented in Table I indicate that the electrons are captured to the $2p_{1/2}$ or $2s_{1/2}$ states rather than the $2p_{3/2}$ state when the projectile energy increases. Moreover, the heavier target Xe shows a stronger energy dependence for this total cross-section ratio.

Stöhlker *et al.* [7] reported a similar phenomenon in U$^{92+} \to$ N$_2$/CH$_4$ collisions with much higher energies of 220–358 MeV/u. The parameter β_{20} of the Lyman-α_1 transition ranges from -0.18 to -0.27. The capture mechanism is attributed to REC. Soon, the alignment mechanism was investigated in detail, e.g., taking into account the contribution of the multipole $M2$ transition, by Surzhykov *et al.* [41]. In addition, Eichler *et al.* [23] calculated the alignment parameter β_{20} of the Lyman-α_1 transition following REC into the $2p_{3/2}$ state of Xe^{54+} ions, without taking into account the cascade feeding contribution and the $E1$-$M2$ interference term. At the projectile energies of 95 and 146 MeV/u, the parameter β_{20}, which is independent of the target species in the REC process, was predicted to be -0.20 and -0.18, respectively. Although the alignment parameters in the present paper fall in the same region as in the previous work [7], and are very close to the theoretical results of Eichler *et al.*, the dominant capture mechanism is not REC, but NRC. This can be realized from Fig. 4, where the shell-selected NRC and REC cross sections are presented. In this figure, the NRC mechanism is evaluated according to the relativistic eikonal approximation [36–38], while the REC channel is calculated by the Stobbe formula, which is based on the nonrelativistic dipole approximation [4,5,42]. Additionally, the K- and L-REC lines are absent in x-ray spectra, as indicated in Fig. 1. This also implies that the REC process is negligible in the present paper. Therefore, the alignment effect studied in the present paper is based on an essentially different capture mechanism to the previous work [7] and demands a detailed alternative theoretical investigation in order to be understood.

It should be noted that electron capture to the higher exciting states (e.g., the $3s$ and $3d$ states) and the following cascade processes contribute to the measured alignment parameters. However, based on the NRC values presented in Fig. 4, the cross sections of electron capture to the M- and N-shells are much smaller than that to the L-shell. Indeed, full range x-ray spectra (e.g., Fig. 1) show that the intensity ratio between the $3p \to 1s$ and the $2p \to 1s$ transitions is around 1/5. Furthermore, more than 85% of the $3p$ state of Xe^{53+*} ions decays directly into the ground state according to calculations of the GRASP program [43,44], which does not affect the present data analysis. However, the $3s$, $3d$, and higher states may involve cascade feeding of the L-subshell levels, which cannot be strictly evaluated. Meanwhile, this correction can be evaluated quantitatively as soon as theoretical state-selective NRC cross sections are available, since the deexcitation branching ratios are accessible (e.g., by the GRASP program [43,44]). Similar calculations had been done in the previous work [7]

TABLE I. The total cross-section ratios $\sigma_{\text{Ly-}\alpha_1}^{\text{total}}/\sigma_{\text{Ly-}\alpha_2(+M1)}^{\text{total}}$ and the alignment parameters $\mathcal{A}_{20}$ of the $2p_{3/2}$ state for the down-charged projectile ions Xe^{53+*} in Xe^{54+} with Kr and Xe collisions. The population ratios of the magnetic substates $m_j = \pm 1/2$ and $\pm 3/2$, which are deduced from the fitting parameter β_{20} according to Eq. (3) with the coefficient [20,41] $\alpha_{\text{eff}} = 0.545$, are also listed.

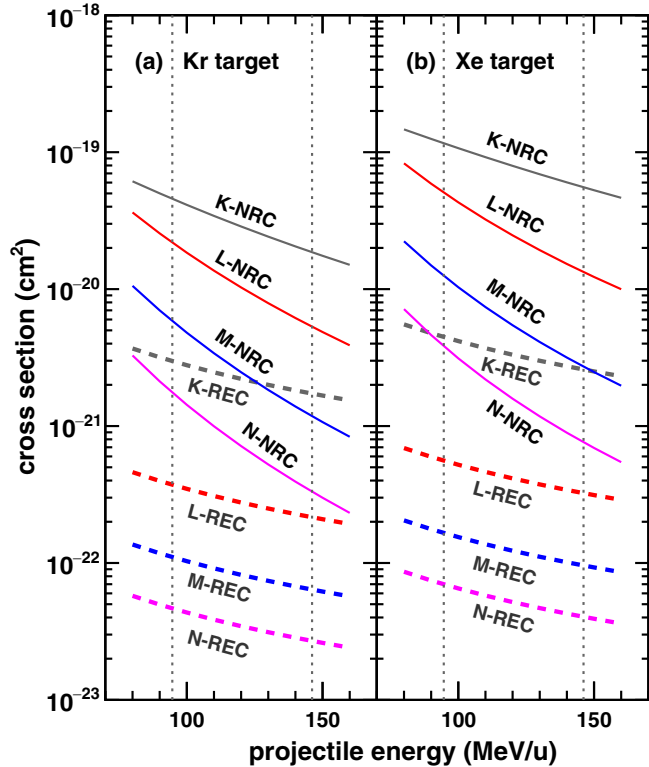| Projectile energy (MeV/u)	Target	$\sigma_{\text{Ly-}\alpha_1}^{\text{total}}/\sigma_{\text{Ly-}\alpha_2(+M1)}^{\text{total}}$	β_{20}	$\mathcal{A}_{20}$	$\sigma(\frac{3}{2}, \pm\frac{1}{2})/\sigma(\frac{3}{2}, \pm\frac{3}{2})$
95	Kr	0.92 ± 0.01	-0.19 ± 0.01	-0.35 ± 0.02	2.08 ± 0.07
	Xe	1.01 ± 0.01	-0.19 ± 0.01	-0.35 ± 0.02	2.08 ± 0.07
146	Kr	0.76 ± 0.01	-0.15 ± 0.01	-0.28 ± 0.02	1.78 ± 0.06
	Xe	0.73 ± 0.01	-0.16 ± 0.02	-0.29 ± 0.04	1.82 ± 0.12

FIG. 4. The K-, L-, M-, and N-shell NRC and REC cross sections to the projectile Xe^{54+} ions from (a) Kr and (b) Xe atoms, for the energy range of 80–160 MeV/u. The solid lines represent the results of the relativistic eikonal approximation for the NRC process [36–38] on the Kr or Xe target. The dashed lines indicate the prediction obtained from the Stobbe formula for the REC process [4,5,42] on the same targets. The projectile energies 95 and 146 MeV/u studied in the present paper are illustrated by dashed vertical lines.

for the REC case. At any rate, the cascade feeding of the $2p_{3/2}$ level leads to isotropic x-ray emission, and decreases the alignment created by direct capture processes. We also note that the double-electron capture probabilities are rather

small for the systems under consideration. This can be seen from the x-ray spectra in Fig. 2.

IV. SUMMARY AND OUTLOOK

In summary, we completed the experimental study of the magnetic-state population in heavy ion-atom collisions between bare xenon ions and neutral krypton or xenon atoms. The measured angular distribution of the Lyman-α_1 radiation following NRC into the $2p_{3/2}$ state of high-Z projectile ions at a middle-energy range (95 and 146 MeV/u) yields a significant negative value of the alignment parameter. It shows that NRC into the $2p_{3/2}$ state populates mostly the $m_j = \pm 1/2$ magnetic substates and the Lyman-α_1 radiation is strongly linearly polarized. The alignment increases with decreasing projectile energy, but is almost independent of the target atoms.

Collisions between fast heavy ions and atoms are very attractive for studying the role of relativistic effects, because of both the high projectile velocity and the strong Coulomb field that the active electrons feel. Moreover, the sensitivity to such effects can be enhanced by measurement of relative angular distributions between the Lyman-α_1 and the Lyman-α_2 transitions, as previous works have demonstrated [7,41]. Hence, stringent tests of our comprehension for electronic dynamics in nonperturbative, relativistic, atomic collisions can be expected in future alignment studies of the excited projectile states via measuring angular distribution of the decay photons.

[1] R. S. Cumbee, P. D. Mullen, D. Lyons, R. L. Shelton, M. Fogle, D. R. Schultz, and P. C. Stancil, Astrophys. J. **852**, 7 (2017).

[2] K. Dennerl, Space Sci. Rev. **157**, 57 (2010).

[3] S. Otranto, R. E. Olson, and P. Beiersdorfer, Phys. Rev. A **73**, 022723 (2006).

[4] J. Eicher and W. E. Meyerhof, *Relativistic Atomic Collisions* (Academic, New York, 1995).

[5] J. Eichler and T. Stöhlker, Phys. Rep. **439**, 1 (2007).

[6] G. Weber, H. Bräuning, A. Surzhykov, C. Brandau, S. Fritzsche, S. Geyer, S. Hagmann, S. Hess, C. Kozhuharov, R. Martin, N. Petridis, R. Reuschl, U. Spillmann, S. Trotsenko, D. F. A. Winters, and T. Stöhlker, Phys. Rev. Lett. **105**, 243002 (2010).

[7] T. Stöhlker, F. Bosch, A. Gallus, C. Kozhuharov, G. Menzel, P. H. Mokler, H. T. Prinz, J. Eichler, A. Ichihara, T. Shirai,

R. W. Dunford, T. Ludziejewski, P. Rymuza, Z. Stachura, P. Swiat, and A. Warczak, Phys. Rev. Lett. **79**, 3270 (1997).

[8] E. H. Pedersen, S. J. Czuchlewski, M. D. Brown, L. D. Ellsworth, and J. R. Macdonald, Phys. Rev. A **11**, 1267 (1975).

[9] L. D. Ellsworth, J. A. Guffey, E. Salzborn, and J. R. Macdonald, Phys. Rev. A **15**, 1438 (1977).

[10] K. Wohrer, F. B. Salah, J. P. Rozet, A. Chetioui, A. Touati, P. Bouisset, D. Vernhet, C. Stephan, and R. Gayet, Nucl. Instrum. Methods Phys. Res., Sect. B **27**, 594 (1987).

[11] D. A. Church, R. A. Kenefick, D. W. Wang, and R. L. Watson, Phys. Rev. A **26**, 3093 (1982).

[12] J. Pálinkás, R. L. Watson, G. J. Pedrazzini, D. A. Church, and R. A. Kenefick, Nucl. Instrum. Methods Phys. Res. A **240**, 498 (1985).

[13] J. Pálinkás, G. J. Pedrazzini, D. A. Church, R. A. Kenefick, C. A. Fulton, R. L. Watson, and D. W. Wang, Phys. Rev. A **31**, 598 (1985).

[14] I. M. Cheshire, Proc. Phys. Soc. **84**, 89 (1964).

[15] A. Chetioui, K. Wohrer, J. P. Rozet, A. Jolly, C. Stephan, D. Belkic, R. Gayet, and A. Salin, J. Phys. B **16**, 3993 (1983).

[16] J. P. Rozet, P. Chevallier, P. Legagneuxpiquemal, A. Chetioui, and C. Stephan, J. Phys. B **18**, 943 (1985).

[17] G. Weber, H. Brauning, A. Surzhykov, C. Brandau, S. Fritzsche, S. Geyer, R. E. Grisenti, S. Hagmann, C. Hahn, R. Hess, S. Hess, C. Kozhuharov, M. Kuhnel, R. Martin, N. Petridis, U. Spillmann, S. Trotsenko, D. F. A. Winters, and T. Stöhlker, J. Phys. B **48**, 144031 (2015).

[18] D. B. Thorn, A. Gumberidze, S. Trotsenko, D. Banas, H. Beyer, C. J. Bostock, I. Bray, W. Chen, R. DuBois, C. J. Fontes, S. Fritzsche, D. V. Fursa, R. Grisenti, S. Geyer, S. Hagmann, S. Hess, M. Hegewald, C. Kozhuharov, R. Martin, I. Orban, N. Petridis, R. Reuschl, A. Simon, U. Spillmann, A. Surzhykov, M. Trassinelli, G. Weber, D. F. A. Winters, N. Winters, H. L. Zhang, and T. Stöhlker, Can. J. Phys. **89**, 513 (2011).

[19] T. Stöhlker, D. Banas, H. Bräuning, S. Fritzsche, S. Geyer, A. Gumberidze, S. Hagmann, S. Hess, C. Kozhuharov, A. Kumar, R. Märtin, B. E. O'Rourke, R. Reuschl, U. Spillmann, A. Surzhykov, S. Tashenov, S. Trotsenko, G. Weber, and D. F. A. Winters, Eur. Phys. J. Spec. Top. **169**, 5 (2009).

[20] T. Stöhlker, D. Banas, S. Fritzsche, A. Gumberidze, C. Kozhuharov, X. Ma, A. Orsic-Muthig, U. Spillmann, D. Sierpowski, A. Surzhykov, S. Tachenov, and A. Warczak, Phys. Scr. **T110**, 384 (2004).

[21] A. Surzhykov, U. D. Jentschura, T. Stöhlker, and S. Fritzsche, Phys. Rev. A **73**, 032716 (2006).

[22] A. Surzhykov, S. Fritzsche, W. D. Sepp, T. Stöhlker, and A. O. Muthig, Nucl. Instrum. Methods Phys. Res., Sect. B **235**, 276 (2005).

[23] J. Eichler, A. Ichihara, and T. Shirai, Phys. Rev. A **58**, 2128 (1998).

[24] S. Zakowicz, Z. Harman, N. Grün, and W. Scheid, Phys. Rev. A **68**, 042711 (2003).

[25] X. Ma, P. H. Mokler, F. Bosch, A. Gumberidze, C. Kozhuharov, D. Liesen, D. Sierpowski, Z. Stachura, T. Stöhlker, and A. Warczak, Phys. Rev. A **68**, 042712 (2003).

[26] P. H. Mokler, T. Kandler, T. Stöhlker, H. Geissel, C. Kozhuharov, P. Rymuza, C. Scheidenberger, Z. Stachura, A. Warczak, and R. W. Dunford, Phys. Scr. **T73**, 247 (1997).

[27] A. Gumberidze, T. Stöhlker, G. Bednarz, F. Bosch, S. Fritzsche, S. Hagmann, D. C. Ionescu, O. Klepper, C. Kozhuharov, A. Krämer, D. Liesen, X. Ma, R. Mann, P. H. Mokler,

D. Sierpowski, Z. Stachura, M. Steck, S. Toleikis, and A. Warczak, Hyperfine Interact. **146**, 133 (2003).

[28] A. Gumberidze, S. Fritzsche, S. Hagmann, C. Kozhuharov, X. Ma, M. Steck, A. Surzhykov, A. Warczak, and T. Stöhlker, Phys. Rev. A **84**, 042710 (2011).

[29] S. Salem, T. Stöhlker, A. Brauning-Demian, S. Hagmann, C. Kozhuharov, D. Liesen, and A. Gumberidze, Phys. Rev. A **88**, 012701 (2013).

[30] T. Ludziejewski, T. Stöhlker, D. C. Ionescu, P. Rymuza, H. Beyer, F. Bosch, C. Kozhuharov, A. Krämer, D. Liesen, P. H. Mokler, Z. Stachura, P. Swiat, A. Warczak, and R. W. Dunford, Phys. Rev. A **61**, 052706 (2000).

[31] J. W. Xia, W. L. Zhan, B. W. Wei, Y. J. Yuan, M. T. Song, W. Z. Zhang, X. D. Yang, P. Yuan, D. Q. Gao, H. W. Zhao, X. T. Yang, G. Q. Xiao, K. T. Man, J. R. Dang, X. H. Cai, Y. F. Wang, J. Y. Tang, W. M. Qiao, Y. N. Rao, Y. He, L. Z. Mao, and Z. Z. Zhou, Nucl. Instrum. Methods Phys. Res. A **488**, 11 (2002).

[32] W. L. Zhan, H. S. Xu, G. Q. Xiao, J. W. Xia, H. W. Zhao, Y. J. Yuan, and H.-C. Group, Nucl. Phys. A **834**, 694c (2010).

[33] C. Shao, D. Yu, X. Cai, X. Chen, K. Ma, J. Evslin, Y. Xue, W. Wang, Y. S. Kozhedub, R. Lu, Z. Song, M. Zhang, J. Liu, B. Yang, Y. Guo, J. Zhang, F. Ruan, Y. Wu, Y. Zhang, C. Dong, X. Chen, and Z. Yang, Phys. Rev. A **96**, 012708 (2017).

[34] X. Cai, R. Lu, C. Shao, F. Ruan, D. Yu, M. Li, W. Zhan, D. K. Torpokov, and D. Nikolenko, Nucl. Instrum. Methods Phys. Res. A **555**, 15 (2005).

[35] C. Shao, R. Lu, X. Cai, D. Yu, F. Ruan, Y. Xue, J. Zhang, D. K. Torpokov, and D. Nikolenko, Nucl. Instrum. Methods Phys. Res., Sect. B **317**, 617 (2013).

[36] R. Anholt and J. Eichler, Phys. Rev. A **31**, 3505 (1985).

[37] J. Eichler, Phys. Rev. A **32**, 112 (1985).

[38] W. E. Meyerhof, R. Anholt, J. Eichler, H. Gould, C. Munger, J. Alonso, P. Thieberger, and H. E. Wegner, Phys. Rev. A **32**, 3291 (1985).

[39] J. Eichler, Nucl. Phys. A **572**, 147 (1994).

[40] J. Eichler, Phys. Rep. **193**, 165 (1990).

[41] A. Surzhykov, S. Fritzsche, A. Gumberidze, and T. Stöhlker, Phys. Rev. Lett. **88**, 153001 (2002).

[42] T. Stöhlker, C. Kozhuharov, P. H. Mokler, A. Warczak, F. Bosch, H. Geissel, R. Moshammer, C. Scheidenberger, J. Eichler, A. Ichihara, T. Shirai, Z. Stachura, and P. Rymuza, Phys. Rev. A **51**, 2098 (1995).

[43] K. G. Dyall, I. P. Grant, C. T. Johnson, F. A. Parpia, and E. P. Plummer, Comput. Phys. Comm. **55**, 425 (1989).

[44] P. Jönsson, X. He, C. Froese Fischer, and I. P. Grant, Comput. Phys. Comm. **177**, 597 (2007).